THE ASTROPHYSICAL JOURNAL, 456:798–810, 1996 January 10

SEISMOLOGY OF η BOOTIS

D. B. GUENTHER
Department of Astronomy and Physics, Saint Mary's University, Halifax, NS, Canada B3H 3C3
AND
P. DEMARQUE
Center for Solar and Space Research, Department of Astronomy, Yale University, New Haven, CT 06520-8101
Received 1995 April 7; accepted 1995 July 14

ABSTRACT

The *p*-mode frequencies recently observed by Kjeldsen and coworkers, along with other observables, are used to determine the mass, age, and helium abundance of η Bootis. We show, by direct application, how the *p*-model frequencies and stellar seismological tools aid in constraining the physical parameters of η Boo. We confirm the existence of mode bumping and discuss how it may be used to refine the estimate of η Boo's age. We describe the effect of the new OPAL equation-of-state tables (Rogers, Swenson, and Iglesias) on the *p*-mode frequencies.

Subject headings: stars: evolution — stars: fundamental parameters — stars: individual (η Bootis) — stars: interiors — stars: oscillations

1. INTRODUCTION

Kjeldsen et al. (1995, hereafter KBVF) have recently announced the detection of Sun-like *p*-mode oscillations on the star η Bootis, and Christensen-Dalsgaard, Bedding, & Kjeldsen (1995, hereafter CBK) have published a companion paper showing that the observed *p*-mode frequencies are compatible with predictions from stellar models. Because η Boo is already a well-studied nearby star with a large parallax, the additional information from seismology presents an excellent opportunity for a detailed theoretical investigation of this star that fully exploits all of the observables, including the oscillation spectrum. In addition, it offers the opportunity to test the ability of seismology, together with stellar evolution theory, to serve as a discriminant of age and distance, with applications to stars more distant than η Boo for which it is not possible to measure a parallax by trigonometric means.

The star η Boo (HR 5235) is classified as G0 IV in the Bright Star Catalogue (Hoffleit & Jaschek 1982). It is a spectroscopic binary (Bertiau 1957; Batten, Fletcher, & McCarthy 1989) with a companion so close that it has not yet been resolved by speckle interferometry; McAllister & Hartkopf (1988) quote an upper bound for the separation of 0".03. In addition, there is a more distant companion which is 113" away. According to Tomkin, Lambert, & Balachandran (1985) and Edvardsson et al. (1993), the metallicity of η Boo is [Fe/H] = 0.19. Its effective temperature has been determined from model atmosphere calculations by Bell & Gustafsson (1989) to be 6050 $\pm$ 60 K. In addition, there is an angular diameter measurement of 2.24 $\pm$ 0.02 mas derived using the infrared flux method (Blackwell & Lynas-Gray 1994).

The weighted mean parallax of η Boo from the Yale Parallax Catalogue (YPC) (van Altena, Lee, & Hoffleit 1995) is given in Table 1, which summarizes the data from several parallaxes. Most of the weight in the YPC compilation has been assigned to the US Naval Observatory measurements by Harrington et al. (1993) because they have very small internal errors. The weighted parallax is 0".0870, with a standard error of 0".0018. The weighted standard error is 0".0034, which reflects the range of the measurements from different sources which are affected by unknown systematic errors. The diameter, the parallax, and the effective temperature listed above yield a luminosity of $L = 9.19\ L_\odot$ for η Boo.

There currently exist several seismological analyses of claimed *p*-mode detections on stars: α Centauri (Demarque, Guenther, & van Altena 1986; Edmonds et al. 1992), ϵ Eridani (Guenther & Demarque 1986; Guenther 1987; Soderblom & Däppen 1989), and Procyon (Guenther & Demarque 1993). Unfortunately, none of the claimed oscillation spectrum identifications have been confirmed. In addition, the theoretically calculated oscillation spectra do not match the observationally claimed spectra. Although the observation of *p*-modes on η Boo by KBVF has not yet been confirmed, either by an independent observation of η Boo or by a successful application of KBVF's technique to another star, it has been shown that the claimed *p*-mode frequencies agree with the *p*-mode frequencies calculated from a simple stellar model of η Boo (CBK). Nevertheless, for the purposes of this study, we shall assume the observations are real and devote our efforts in this paper primarily to applying the tools of stellar seismology to η Boo. We stress that the very fact that we are able to perform successfully a detailed analysis of the observations lends support to their validity.

In § 2, we describe the stellar evolution sequences. Our basic approach is, first, to use all the observables other than the *p*-modes to constrain stellar models of η Boo in the conventional way. Most crucial among the observables are the metallicity Z from spectroscopy and the parallax from astrometry. Given these two input parameters, one then finds a family of possible models for η Boo (i.e., those which satisfy η Boo's metallicity and position in the theoretical H-R diagram). Each of these possible solutions is characterized by three parameters: the helium mass fraction Y, the mass M, and the age of the model. Note that if one were able to determine precisely any one of these three parameters independently, the other two would be uniquely determined by the grid of evolutionary models. Unfortunately, it is not possible to measure Y spectroscopically with any reliability in a G0 IV star. Although η Boo has a faint binary companion, the orbit of the system (and

TABLE 1

YPC LISTING FOR η BOO

YPC	Observatory[a]	Standard Error	PIABS[b]	Weight
3175.00.....	ALL	0".0084	0".1026	14.1
3175.00.....	MCC	0.0150	0.1130	4.4
3175.00.....	USN	0.0019	0.0858	277.0
3175.00.....	YPC	0.0034[c]	0.0870	...

[a] ALL—Allegheny Observatory; MCC—McCormick Observatory; USN—US Naval Observatory; YPC—Yale Parallax Catalogue weighted parallax.

[b] PIABS—absolute parallax (arcsec).

[c] Weighted standard error.

therefore the masses of its components) has yet to be determined. Finally, there is no way to evaluate η Boo's age independently by conventional means with the precision required. Therefore, this is as far as the conventional analysis can take us.

In § 3, with the help of a detailed grid of evolutionary models, we show how the p-mode oscillation spectrum can be used to constrain the parameter space for η Boo and to derive additional, previously inaccessible, information about the star. Specifically, we show that it is possible to fix uniquely which of the family of stellar models, each characterized by a triplet (Y, M, and age) as derived in the previous section, yields stellar models whose predicted p-modes match η Boo's observed p-mode frequencies. In other words, the p-mode spectrum serves here as a powerful discriminant among the possible models for η Boo. We also present the results of stellar model calculations of η Boo that use the new OPAL equation-of-state tables (Rogers, Swenson, & Iglesias 1995).

The analysis is necessarily complicated by errors associated with each input parameter. Estimates of these errors are taken into account in the discussions of §§ 2 and 3. Because of these unavoidable uncertainties, and also as a check of internal consistency, redundancies in the data are particularly valuable. We note, in particular, that additional information about evolutionary stage (or age) can be derived from the existence of mode bumping in η Boo's oscillation spectrum.

In the study of Galactic nucleosynthesis, i.e., the study of the chemical evolution of our Galaxy, it is convenient to characterize the helium abundance of a star by the Galactic-enrichment parameter (Bressan, Chiosi, & Fagotto 1994), defined here with respect to the Sun as $\Delta Y/\Delta Z \equiv (Y_* - Y_\odot)/(Z_* - Z_\odot)$. We demonstrate that even the broad limits set on Y by the $\Delta Y/\Delta Z$ of Galactic nucleosynthesis, when applied jointly with the p-mode constraint, significantly restrict the acceptable range for η Boo's parallax. Remarkably, these limits put more stringent constraints on η Boo's distance than the best presently available trigonometric parallax.

2. THE MODELS

2.1. *Model Calculation*

All of the models presented here were evolved from the zero-age main sequence (ZAMS) in approximately 300 (necessarily unequal) time steps using the Yale Stellar Evolution Code (YREC) (Guenther, Jaffe, & Demarque 1989). Each model contains approximately 1800 shells divided equally among the interior, the envelope (outer 1% of the mass), and the atmosphere.

The constitutive physics used to construct models of η Boo is very nearly identical to that used to construct standard solar models (Guenther et al. 1992). The most significant difference is the use of a gray atmosphere in the Eddington approximation rather than a detailed fit to the Sun's atmosphere. The nuclear energy generation routines are from Bahcall & Pinsonneault (1992), and the cross sections are from Bahcall's Neutrino Astrophysics (Bahcall 1989). The cross section of the PP reaction, the ^{7}Be-proton capture reaction, and the hep reaction (M. Pinsonneault 1995, private communication) have been updated to current values. For most of the models YREC's standard equation-of-state routines were used with the Debye-Hückel correction (Clayton 1968; Cox & Giuli 1968; Landau & Lifshitz 1959, § 78; Bahcall, Bahcall, & Shaviv 1968; Guenther et al. 1992). The Debye-Hückel correction is probably inadequate in the dense cores of stars (Däppen 1995, private communication). To see how the new OPAL equation-of-state tables (F. J. Rogers 1995, private communication; Rogers et al. 1995) affect the results, we have also calculated a set of models using the OPAL equation-of-state tables. For a detailed discussion of the OPAL (and MHD) equation of state, within the context of the standard solar model, see Guenther, Kim, & Demarque (1995). OPAL opacities (Iglesias & Rogers 1991; Rogers & Iglesias 1994) were used, except at low temperatures, where we switched to the Kurucz opacities (Kurucz 1991). We chose the Anders & Grevesse (1989) mixture of elements with meteoritic iron abundance. The effects of diffusion and rotation are not included in any of the model calculations presented here, but will probably be considered at a future time.

2.2. *Constraints from Stellar Evolution*

The constraints on η Boo from stellar evolution are best described in the theoretical H-R diagram (see Fig. 1). The position of η Boo and its error box in the theoretical H-R diagram, together with what we know about its metallicity, provides us with what, until the advent of seismology, has been the primary way of determining its evolutionary status. The size of the error box shown is set by the uncertainties in $T_{\rm eff}$ (Bell & Gustafsson 1989) and the infrared flux diameter measurement (Blackwell & Lynas-Gray 1994) used to derive the luminosity. We account for errors in parallax in our analysis, but they have not been folded into the error bars for η Boo's position in the H-R diagram, since they primarily shift the error box up and down in luminosity. Observation also provides the metallicity of η Boo with [Fe/H] = 0.19, which gives $Z = 0.03$ for $Z_\odot = 0.0188$ (Guenther et al. 1992). There is also an error bar attached to Z which we shall account for in our analysis.

For a given value of Z and parallax, there is, in general, a family of models whose evolutionary path passes through η Boo's position in the H-R diagram. In our analysis, we identify individual members by their mass, but one is free to distinguish the family members by their age or helium abundance. In Figure 1 we show two different tracks (of distinct mass and similar parallax and Z) that pass through the center of η Boo's position box in the H-R diagram. The range of possible values of M, Y, and age for a stellar model η Boo increases when one also considers the error bars associated with the observed position in the H-R diagram and the error bars associated with metallicity and parallax determination. Even in the favorable case of η Boo, for which we have a relatively good parallax, stellar evolution alone cannot uniquely determine the physical properties of the star.

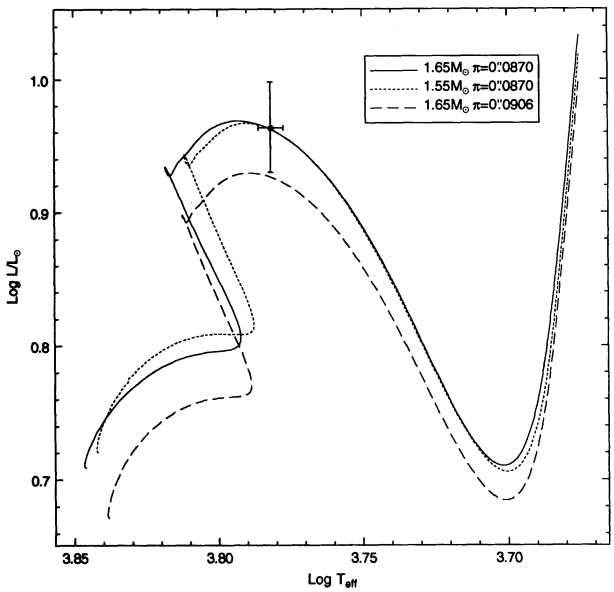

FIG. 1.—Evolutionary tracks corresponding to several models of η Bootis are shown in the theoretical H-R diagram. The data point with error bars locates the position of η Boo in the H-R diagram assuming that the parallax of η Boo is $\pi = 0''.0870$.

All of the models presented in this work, for a given parallax and Z, lie at the center of the H-R diagram position of η Boo. Because different parallaxes imply different luminosities for η Boo, the position of η Boo will shift up and down in luminosity depending on the parallax used (see Table 7). A three-dimensional parameter space was calculated spanning different Z, parallax, and mass. We have not directly examined ranges of luminosity because the luminosity sensitivity is conveniently revealed by examining a range of parallaxes (see third track in Fig. 1). The sensitivity of the models and the p-mode frequencies to the error in $T_{\rm eff}$ is also not explored explicitly because the $T_{\rm eff}$ sensitivity can be inferred from the luminosity sensitivity and the fact that, to first order, $\Delta\nu/\nu = -\Delta R/R$.

All of the tracks in the grid, except as noted, were calculated with the same mixing-length parameter, $\alpha = 1.7$, which is the calibrated value from a standard solar model that uses the same input physics used to construct the models of η Boo. We have also examined a family of models whose mixing-length parameter is $\alpha = 2.0$.

We constructed models for $Z = 0.02$, 0.03, and 0.04. For each value of Z we constructed models for parallaxes ranging from $0''.0858$ to $0''.0918$, and for each Z and parallax we constructed models with masses ranging from 1.4 to 1.8 $M_\odot$. Additionally, a set of models were calculated using the OPAL equation-of-state tables for $Z = 0.03$. Characteristics of the final models for all of the evolutionary sequences calculated are summarized in Tables 2–6. Again, we stress that for a given parallax all of the models lie in exactly the same position in the H-R diagram.

The parameter $\Delta Y/\Delta Z$, which we associate with each Y and is evaluated here with respect to the Sun, is fundamental in studies of galaxy evolution and the chemical enrichment of stellar poplations by nucleosynthesis. The value of $\Delta Y/\Delta Z$ is believed to be ~ 3 for the lowest metallicity populations. It is ~ 2.6 for the Sun. Recent population models of galaxies favor 2.5 for $\Delta Y/\Delta Z$ (Bressan et al. 1994). This parameter, therefore, constrains the acceptable range for the helium content of η Boo. Providing a model of η Boo with a value of Y that is incompatible with other Galactic data, while of academic interest, raises more questions than it answers when placed in the broader astronomical context. Consider, for example, models of η Boo with $Z = 0.03$, $\alpha = 1.7$, and $\pi = 0''.0870$ (see Table 2); then $\Delta Y/\Delta Z = 2$–3 constrains the mass of η Boo to 1.55–1.66 $M_\odot$. We will make further use of $\Delta Y/\Delta Z$ in our analysis.

TABLE 2

MODEL CHARACTERISTICS ($\alpha = 1.7$; $Z = 0.03$)

Parallax	Mass ($M_\odot$)	X	$\Delta Y/\Delta Z$	Age (Gyr)	Mass C.Z. ($M_\odot$)	log $T_{\rm eff}$	$M_{\rm bol}$	log $(L/L_\odot)$	log $(R/R_\odot)$	log g	$\Delta\nu$ (μHz)	$\nu(0,21)$ (μHz)	$\nu(0,20)$ (μHz)	$\nu(2,19)$ (μHz)
0".0858.....	1.60	0.69223	1.67	2.1806	0.00000	3.78119	2.35684	0.97327	0.44805	3.746	37.49	851.36	814.45	811.34
0.0858.....	1.65	0.71377	−0.26	2.2485	0.00000	3.78203	2.34849	0.97661	0.44805	3.759	38.06	864.60	827.08	823.98
0.0858.....	1.70	0.73599	−2.24	2.3396	0.00000	3.78233	2.34547	0.97781	0.44805	3.772	38.63	878.13	840.00	836.82
0.0858.....	1.75	0.75776	−4.18	2.4088	0.00183	3.78207	2.34800	0.97680	0.44805	3.785	39.21	891.54	852.83	849.60
0.0858.....	1.80	0.77929	−6.11	2.4898	0.00205	3.78202	2.34856	0.97658	0.44805	3.797	39.77	904.76	865.45	862.18
0.0870.....	1.55	0.67451	3.25	2.1679	0.00000	3.78143	2.38465	0.96214	0.44202	3.744	37.67	855.04	819.36	817.12
0.0870.....	1.60	0.69708	1.23	2.2378	0.00000	3.78160	2.38292	0.96283	0.44202	3.758	38.27	869.29	831.58	828.46
0.0870.....	1.65	0.72005	−0.82	2.3449	0.00174	3.78147	2.38422	0.96231	0.44202	3.771	38.87	883.44	845.13	841.94
0.0870.....	1.70	0.74053	−2.65	2.3803	0.00176	3.78225	2.37644	0.96542	0.44202	3.784	39.44	896.80	857.86	854.62
0.0870.....	1.75	0.76389	−4.73	2.4981	0.00207	3.78154	2.38355	0.96258	0.44202	3.797	40.05	910.97	871.42	868.11
0.0882.....	1.50	0.65737	4.78	2.1795	0.00000	3.78192	2.40941	0.95223	0.43608	3.742	37.79	858.05	820.77	817.68
0.0882.....	1.55	0.67945	2.81	2.2308	0.00000	3.78150	2.41358	0.95057	0.43608	3.756	38.44	873.13	835.23	832.09
0.0882.....	1.60	0.70235	0.76	2.3289	0.00161	3.78164	2.41220	0.95112	0.43608	3.770	39.06	887.63	849.12	845.91
0.0882.....	1.65	0.72459	−1.22	2.3883	0.00182	3.78153	2.41335	0.95066	0.43608	3.783	39.68	902.01	862.88	859.61
0.0882.....	1.70	0.74708	−3.23	2.5037	0.00184	3.78219	2.40671	0.95332	0.43608	3.796	40.26	915.84	876.07	873.37
0.0894.....	1.45	0.63854	6.46	2.1517	0.00000	3.78185	2.43947	0.94021	0.43020	3.739	37.91	860.73	823.28	820.19
0.0894.....	1.50	0.66115	4.44	2.2228	0.00000	3.78195	2.43852	0.94059	0.43020	3.753	38.56	876.00	837.92	834.73
0.0894.....	1.55	0.68485	2.33	2.3069	0.00160	3.78139	2.44411	0.93836	0.43020	3.768	39.23	891.34	852.67	849.43
0.0894.....	1.60	0.70688	0.36	2.3767	0.00166	3.78181	2.43987	0.94005	0.43020	3.781	39.85	905.90	866.58	863.29
0.0906.....	1.45	0.64318	6.05	2.2227	0.00000	3.78161	2.47089	0.92765	0.42441	3.750	38.68	878.44	840.26	837.05
0.0906.....	1.50	0.66611	4.00	2.2971	0.00000	3.78211	2.46589	0.92964	0.42441	3.765	39.34	893.89	855.03	851.75
0.0906.....	1.55	0.69000	1.87	2.3834	0.00167	3.78124	2.47451	0.92619	0.42441	3.779	40.02	909.63	870.19	866.87
0.0906.....	1.60	0.71268	−0.16	2.4621	0.00181	3.78145	2.47245	0.92702	0.42441	3.793	40.67	924.68	884.57	881.18

TABLE 3

MODEL CHARACTERISTICS ($\alpha = 2.0$; $Z = 0.03$)

Parallax	Mass ($M_\odot$)	X	$\Delta Y/\Delta Z$	Age (Gyr)	Mass C.Z. ($M_\odot$)	log $T_{\rm eff}$	$M_{\rm bol}$	log ($L/L_\odot$)	log ($R/R_\odot$)	log g	$\Delta\nu$ (μHz)	ν(0,21) (μHz)	ν(0,20) (μHz)	ν(2,19) (μHz)
0".0858.....	1.60	0.68311	2.48	2.0792	0.00722	3.78229	2.34582	0.97767	0.44805	3.746	37.73	857.41	820.35	817.24
0.0858.....	1.65	0.70659	0.38	2.1863	0.00857	3.78140	2.35472	0.97411	0.44805	3.759	38.33	871.71	833.93	830.45
0.0858.....	1.70	0.72635	−1.38	2.2063	0.00892	3.78187	2.35010	0.97596	0.44805	3.772	38.91	885.13	846.73	843.21
0.0858.....	1.75	0.74886	−3.39	2.3090	0.00967	3.78182	2.35055	0.97578	0.44805	3.785	39.48	898.67	859.64	856.43
0.0870.....	1.55	0.66665	3.95	2.0830	0.00766	3.78145	2.38446	0.96222	0.44202	3.744	37.92	861.73	824.45	821.33
0.0870.....	1.60	0.69000	1.87	2.1860	0.00779	3.78213	2.37762	0.96495	0.44202	3.758	38.53	875.97	838.05	835.16
0.0870.....	1.65	0.71124	−0.03	2.2256	0.00900	3.78123	2.38662	0.96135	0.44202	3.771	39.14	890.34	851.71	848.82
0.0870.....	1.70	0.73320	−1.99	2.3227	0.00923	3.78177	2.38117	0.96353	0.44202	3.784	39.73	904.15	864.89	861.64
0.0882.....	1.50	0.64961	5.47	2.0881	0.00681	3.78203	2.40830	0.95268	0.43608	3.742	38.06	864.79	827.44	824.32
0.0882.....	1.55	0.67332	3.36	2.1823	0.00766	3.78178	2.41081	0.95168	0.43608	3.756	38.71	879.87	841.78	838.82
0.0882.....	1.60	0.69327	1.57	2.2210	0.00784	3.78236	2.40505	0.95398	0.43608	3.770	39.32	894.17	855.42	852.25
0.0882.....	1.65	0.71647	−0.50	2.3036	0.00855	3.78214	2.40723	0.95311	0.43608	3.783	39.94	908.73	869.30	866.02
0.0894.....	1.45	0.63233	7.02	2.1045	0.00669	3.78181	2.43991	0.94004	0.43020	3.739	38.19	867.41	829.95	826.30
0.0894.....	1.50	0.65432	5.05	2.1485	0.00702	3.78222	2.43581	0.94168	0.43020	3.753	38.84	882.68	844.51	841.43
0.0894.....	1.55	0.67732	3.00	2.2328	0.00821	3.78133	2.44472	0.93811	0.43020	3.768	39.50	898.24	859.30	856.11
0.0894.....	1.60	0.70000	0.97	2.3124	0.00877	3.78165	2.44149	0.93940	0.43020	3.781	40.13	913.15	873.52	870.23

TABLE 4

MODEL CHARACTERISTICS ($\alpha = 1.7$; $Z = 0.02$)

Parallax	Mass ($M_\odot$)	X	$\Delta Y/\Delta Z$	Age (Gyr)	Mass C.Z. ($M_\odot$)	log $T_{\rm eff}$	$M_{\rm bol}$	log ($L/L_\odot$)	log ($R/R_\odot$)	log g	$\Delta\nu$ (μHz)	ν(0,21) (μHz)	ν(0,20) (μHz)	ν(2.19) (μHz)
0".0870.....	1.55	0.72485	−1.25	2.3561	0.00295	3.78139	2.38506	0.96198	0.44202	3.744	37.80	859.31	822.06	819.25
0.0870.....	1.60	0.74887	−3.39	2.4500	0.00311	3.78167	2.38220	0.96312	0.44202	3.758	38.40	873.51	835.57	832.47
0.0870.....	1.65	0.77148	−5.41	2.5174	0.00354	3.78135	2.38547	0.96181	0.44202	3.771	39.01	887.76	849.11	845.93
0.0870.....	1.70	0.79494	−7.50	2.6370	0.00352	3.78230	2.37595	0.96562	0.44202	3.784	39.58	901.32	862.05	858.77
0.0882.....	1.55	0.73077	−1.77	2.4462	0.00298	3.78156	2.41300	0.95080	0.43608	3.756	38.57	877.27	838.20	836.06
0.0882.....	1.60	0.75369	−3.82	2.5214	0.00308	3.78214	2.40724	0.95310	0.43608	3.770	39.19	891.65	852.89	849.67
0.0882.....	1.65	0.77735	−5.93	2.6147	0.00348	3.78187	2.40995	0.95202	0.43608	3.783	39.80	906.25	866.77	863.48
0.0882.....	1.70	0.80126	−8.07	2.7163	0.00408	3.78128	2.41580	0.94968	0.43608	3.796	40.42	920.78	880.60	877.24
0.0894.....	1.45	0.68865	1.99	2.3625	0.00254	3.78164	2.44165	0.93934	0.43020	3.739	38.06	865.01	827.60	824.55
0.0894.....	1.50	0.71234	−0.13	2.4411	0.00277	3.78187	2.43931	0.94028	0.43020	3.753	38.71	880.21	842.07	840.31
0.0894.....	1.55	0.73546	−2.19	2.5137	0.00288	3.78232	2.43480	0.94208	0.43020	3.768	39.35	895.21	856.35	853.09
0.0894.....	1.60	0.76004	−4.39	2.6246	0.00315	3.78230	2.43497	0.94201	0.43020	3.781	39.99	910.23	870.63	867.30
0.0906.....	1.40	0.67020	3.63	2.3815	0.00242	3.78165	2.47045	0.92782	0.42441	3.735	38.14	866.71	829.28	826.15
0.0906.....	1.45	0.69396	1.51	2.4533	0.00260	3.78196	2.46739	0.92904	0.42441	3.750	38.82	882.52	844.33	841.11
0.0906.....	1.50	0.71794	−0.63	2.5434	0.00279	3.78219	2.46505	0.92998	0.42441	3.765	39.49	898.14	859.18	855.90
0.0906.....	1.55	0.74135	−2.72	2.6156	0.00300	3.78233	2.46368	0.93053	0.42441	3.779	40.14	913.59	873.88	870.51

TABLE 5

MODEL CHARACTERISTICS ($\alpha = 1.7$; $Z = 0.04$)

Parallax	Mass ($M_\odot$)	X	$\Delta Y/\Delta Z$	Age (Gyr)	Mass C.Z. ($M_\odot$)	log $T_{\rm eff}$	$M_{\rm bol}$	log ($L/L_\odot$)	log ($R/R_\odot$)	log g	$\Delta\nu$ (μHz)	ν(0,21) (μHz)	ν(0,20) (μHz)	ν(2,19) (μHz)
0".0858.....	1.65	0.67678	3.05	2.1480	0.00000	3.78123	2.35644	0.97343	0.44805	3.759	37.99	862.63	824.87	821.74
0.0858.....	1.70	0.69689	1.25	2.2100	0.00000	3.78195	2.34929	0.97628	0.44805	3.772	38.55	875.75	837.45	834.33
0.0858.....	1.75	0.71795	−0.63	2.2682	0.00000	3.78181	2.35066	0.97574	0.44805	3.785	39.12	889.22	850.39	847.19
0.0858.....	1.80	0.73849	−2.46	2.3413	0.00000	3.78192	2.34959	0.97617	0.44805	3.797	39.68	902.42	863.05	859.78
0.0870.....	1.60	0.65954	4.59	2.1309	0.00000	3.78175	2.38142	0.96343	0.44202	3.758	38.17	866.79	828.76	825.55
0.0870.....	1.65	0.68122	2.65	2.2022	0.00000	3.78151	2.38378	0.96249	0.44202	3.771	38.78	880.93	842.36	839.28
0.0870.....	1.70	0.70215	0.78	2.2688	0.00000	3.78178	2.38115	0.96354	0.44202	3.784	39.37	894.72	855.60	852.37
0.0870.....	1.75	0.72418	−1.19	2.3577	0.00000	3.78127	2.38618	0.96153	0.44202	3.797	39.97	908.64	868.99	865.70
0.0882.....	1.55	0.64237	6.12	2.1189	0.00000	3.78163	2.41234	0.95106	0.43608	3.756	38.34	870.53	832.27	829.04
0.0882.....	1.60	0.66471	4.14	2.1974	0.00000	3.78133	2.41527	0.94989	0.43608	3.770	38.97	885.34	846.52	843.36
0.0882.....	1.65	0.68608	2.22	2.2612	0.00000	3.78141	2.41452	0.95019	0.43608	3.783	39.59	899.56	860.19	856.95
0.0894.....	1.50	0.62512	7.66	2.1108	0.00000	3.78133	2.44475	0.93810	0.43020	3.753	38.49	873.61	835.18	831.92
0.0894.....	1.55	0.64701	5.70	2.1817	0.00000	3.78174	2.44060	0.93976	0.43020	3.768	39.13	888.64	849.59	846.38
0.0894.....	1.60	0.66877	3.76	2.2637	0.00000	3.78171	2.44087	0.93965	0.43020	3.781	39.76	903.56	863.93	860.67

TABLE 6

MODEL CHARACTERISTICS ($\alpha = 1.7$; $Z = 0.03$; OPAL Equation of State)

Parallax	Mass ($M_\odot$)	X	$\Delta Y/\Delta Z$	Age (Gyr)	Mass C.Z. ($M_\odot$)	log $T_{\rm eff}$	$M_{\rm bol}$	log $(L/L_\odot)$	log $(R/R_\odot)$	log g	$\Delta\nu$ (μHz)	$\nu(0,21)$ (μHz)	$\nu(0,20)$ (μHz)	$\nu(2,19)$ (μHz)
0.0882.....	1.60	0.70240	0.76	2.3236	0.00180	3.78199	2.40870	0.95252	0.43608	3.770	39.04	887.26	848.78	845.51
0.0882.....	1.65	0.72440	−1.21	2.3905	0.00202	3.78199	2.40870	0.95252	0.43608	3.783	39.65	901.62	862.52	859.20
0.0894.....	1.50	0.66140	4.42	2.2302	0.00157	3.78159	2.44213	0.93915	0.43020	3.753	38.56	878.09	839.14	835.86
0.0894.....	1.55	0.68440	2.37	2.3118	0.00173	3.78191	2.43895	0.94042	0.43020	3.768	39.20	890.83	852.19	848.90
0.0894.....	1.60	0.70690	0.36	2.3670	0.00201	3.78163	2.44175	0.93930	0.43020	3.781	39.85	905.78	866.53	863.20
0.0906.....	1.45	0.64300	6.06	2.2203	0.00144	3.78178	2.46912	0.92835	0.42441	3.750	38.65	878.02	839.87	836.60
0.0906.....	1.50	0.66610	4.00	2.2853	0.00161	3.78194	2.46750	0.92900	0.42441	3.765	39.33	893.66	854.87	851.55
0.0906.....	1.55	0.68915	1.94	2.3646	0.00187	3.78168	2.47015	0.92794	0.42441	3.779	40.00	909.25	869.84	866.47
0.0918.....	1.40	0.62470	7.70	2.2240	0.00137	3.78171	2.49839	0.91664	0.41870	3.746	38.73	879.59	841.34	838.05
0.0918.....	1.45	0.64825	5.59	2.2983	0.00162	3.78138	2.50166	0.91543	0.41870	3.762	39.44	895.90	857.05	853.71
0.0918.....	1.50	0.67089	3.57	2.3682	0.00162	3.78235	2.49205	0.91918	0.41870	3.776	40.10	911.42	871.85	868.44

2.3. *Model Results*

A quick review of the model characteristics listed in Tables 2–6 and Figure 1 reveals that η Boo, according to stellar evolutionary constraints, is a 1.4–1.8 $M_\odot$ star with an age between 2.0 and 2.5 Gyr. Its convection zone is very thin. It has a pure helium core, having exhausted its central hydrogen. All of these are characteristics of a star in the subgiant phase of evolution, in its journey from the main-sequence turnoff to the base of the giant branch. These numbers will be significantly constrained when the observed p-mode oscillation spectrum is considered.

Some of the models do not have convective envelopes. We believe that η Boo has a convective envelope, for the following reasons:

1. There is spectroscopic evidence in stars like η Boo for photospheric convection at small optical depth.
2. In the case of the Sun, we have strong evidence that it is the turbulent convection in the superadiabatic layer, located near the surface, that drives the oscillations. If this driving mechanism is correct, we must conclude that a very thin convection zone extending into the photosphere is responsible for the p-modes observed on η Boo.

Therefore, we conclude that the models that do not have convective envelopes, or at least their surface layers, are not accurate representations of η Boo.

We know that the surface layers of η Boo are not being modeled accurately, since radiative equilibrium is assumed above the photosphere (implicit in the use of the Eddington approximation). Additionally, there are possibly errors in the low-temperature opacities which are large enough to affect the atmospheric models significantly. The nonzero slope in the frequency-difference plots, described below, is further evidence that the surface-layer modeling needs to be improved.

2.4. *OPAL Equation of State*

Comparing the data for the models calculated using YREC's standard equation-of-state routines (Table 2) and models calculated using the more sophisticated OPAL equation-of-state routines (Table 6) reveals that the new OPAL equation of state has very little effect on the model and its p-mode frequencies. The OPAL equation of state slightly increases the convection zone depth.

We consider the models calculated using the OPAL equation of state our "best" models, in the sense that the interior structure is determined using the best interior physics we currently have.

3. THE MODES

3.1. *p-Mode Calculation*

The η Boo stellar models served as input into Guenther's nonradial nonadiabatic stellar pulsation program (Guenther 1994), where the p-mode frequencies corresponding to the modes identified by KBVF were calculated. The nonadiabatic calculation only considers radiative processes (Eddington approximation) and neglects what may be important corrections owing to turbulent convection (Balmforth 1992a, b, c). The coupling of turbulent convection with the p-modes perturbs the frequencies of the modes. Because the strength of the coupling is strongest in the superadiabatic layer (as are the radiative effects), the frequency spacings between the modes, which are predominantly sensitive to the surface layers, are affected.

We have no direct way of judging the quality of the p-mode frequency determinations for η Boo, but we note that for the standard solar model with the input physics used here and a similar nonadiabatic p-mode calculation, we can reproduce the observed frequencies of the Sun to within $\pm 0.3\%$. The discrepancy between the standard solar model and the observed frequencies is reduced by a factor of 2 when the OPAL equation of state (F. J. Rogers 1995, private communication) *and* diffusion of helium are included in the standard solar model calculation (Guenther et al. 1995). Because of the modeling difficulties associated with the very shallow convection zone, we have not included the diffusion in the calculation of the models of η Boo at this time. Based on the accuracy of standard solar-model p-mode frequency determinations and the error associated with using a gray atmosphere in the Eddington approximation (Guenther et al. 1992), we estimate that our p-mode frequency calculations are accurate to ± 5 μHz or $\sim \pm 0.6\%$.

3.2. *General p-Mode Results*

In Figures 2–6, we plot the frequency differences (model minus observed) against the observed frequencies (KBVF) for the models listed in Tables 2–6. In these plots, a perfect match between model and observation would correspond to a horizontal line of points at 0 μHz. Lines connect the common l-values of the modes. The longest line corresponds to $l = 1$, and, of course, the two shorter lines to $l = 0$ and 2. We have grouped together, in one plot, the frequency differences for a reasonable range of masses at a given parallax. The adjacent plots correspond to different assumed parallaxes, hence, differ-

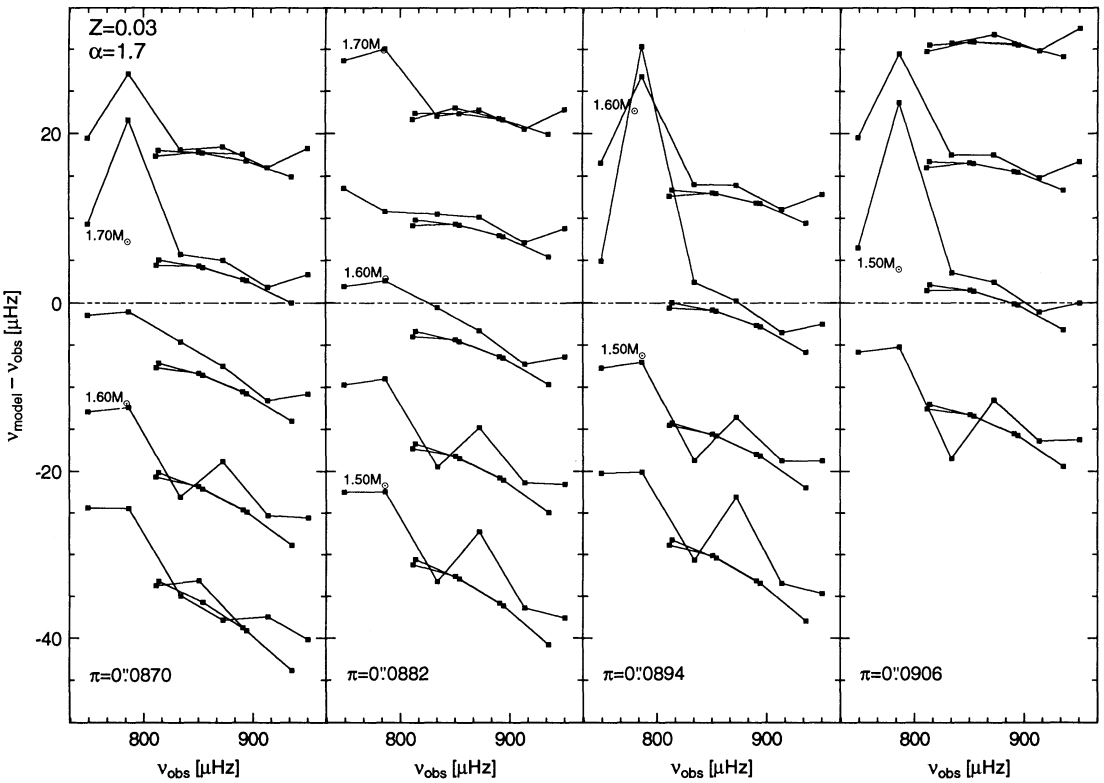

FIG. 2.—The p-mode frequency differences (model minus observed) are plotted opposite the observed frequencies for a variety of η Boo stellar models. All of the models were constructed with $Z = 0.03$ and $\alpha = 1.7$. The masses of some of the models are indicated near the left of the frequency-difference curves. The assumed parallaxes for the models are shown in the lower left corner of each plot.

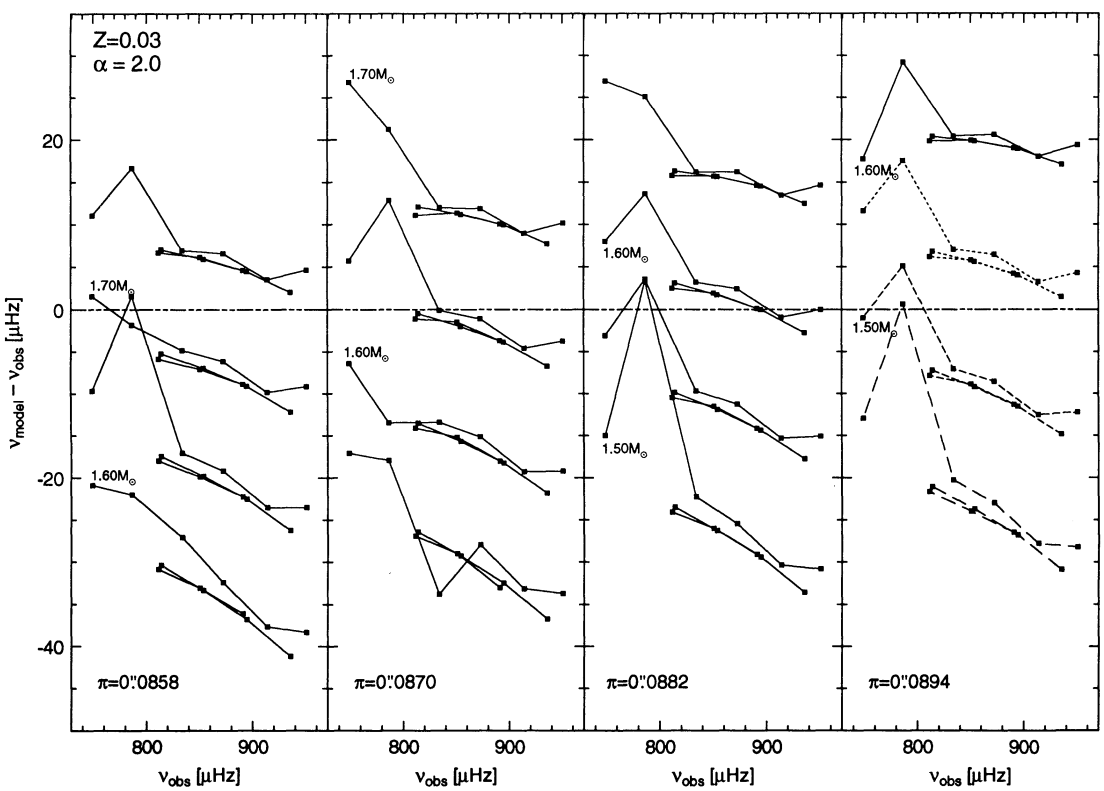

FIG. 3.—Similar to Fig. 2, except that models were constructed with $Z = 0.03$ and $\alpha = 2.0$

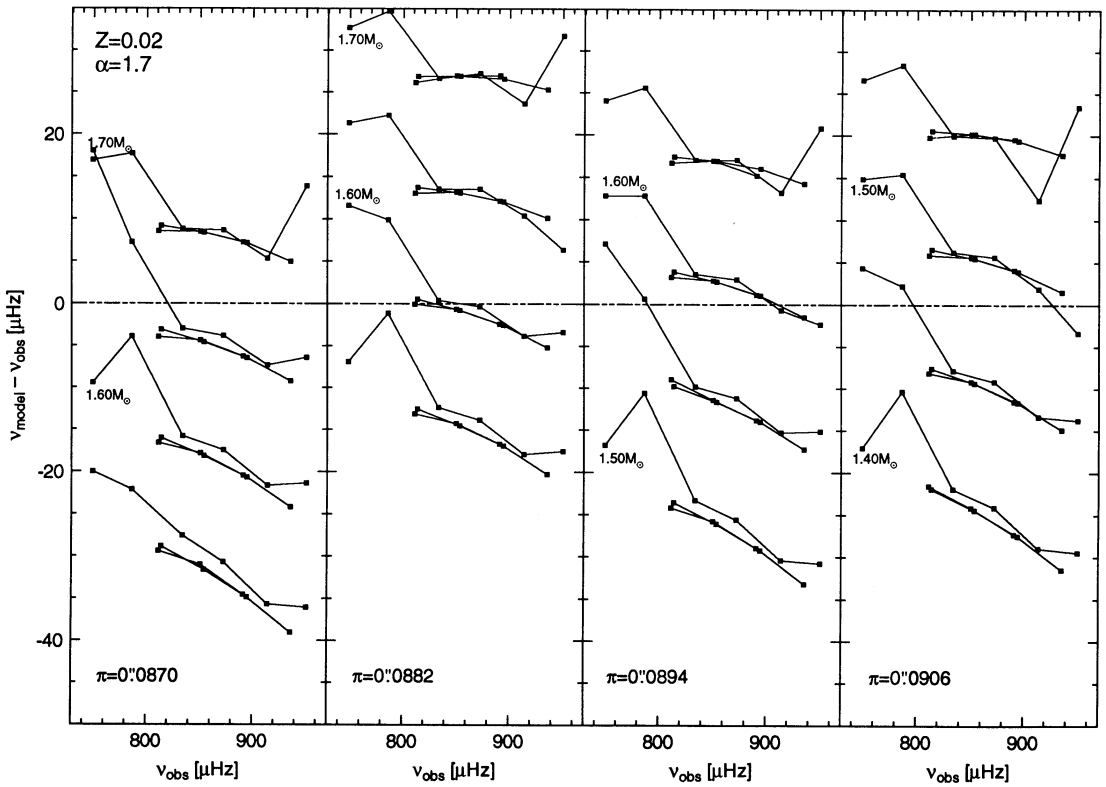

FIG. 4.—Similar to Fig. 2, except that models were constructed with $Z = 0.02$ and $\alpha = 1.7$

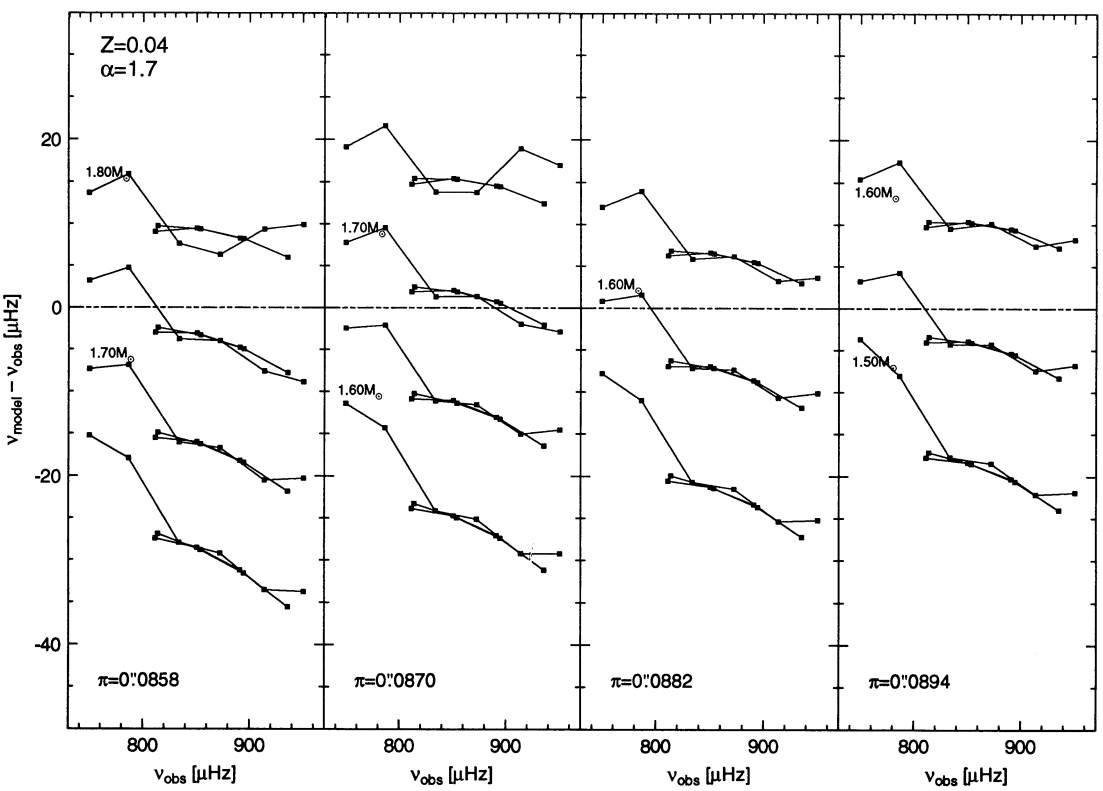

FIG. 5.—Similar to Fig. 2, except that models were constructed with $Z = 0.04$ and $\alpha = 1.7$

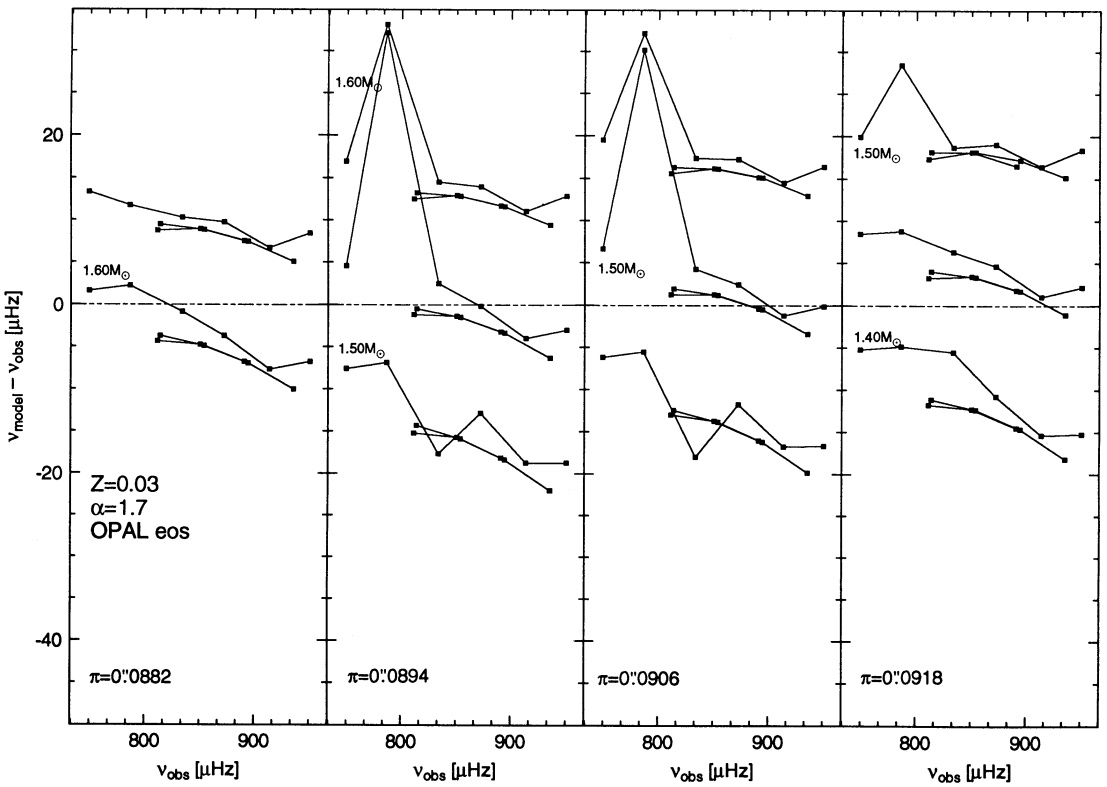

FIG. 6.—Similar to Fig. 2, except that models were constructed using the latest OPAL equation-of-state routines (with $Z = 0.03$ and $\alpha = 1.7$)

ent luminosities (see Table 7). The models in Figures 2 and 7 (Table 2) represent our benchmark models that are based on the observed value for Z and the (standard solar model) tuned value for α. We will compare the other models, shown in the other figures, to the benchmark models. Regardless, we consider the models in Figures 6 and 11 (Table 6) that are also based on the observed value for Z and the tuned value for α, but are calculated using the OPAL equation-of-state routines, to be our best models (they are not significantly different from the benchmark models.).

What is most remarkable about the plots in Figures 2–6 is that even though all the models represented are identical with respect to the stellar evolutionary constraints of effective temperature, luminosity, and metallicity, they all have distinct oscillation spectra. There is no doubt, when considering these figures, that stellar seismology can provide useful additional information about the physical characteristics of stars.

For a given parallax, the best model and corresponding mass are easily identifiable. For example, in Figure 2, corresponding to $Z = 0.03$ and $\alpha = 1.7$ (standard values), the best model for an assumed parallax $\pi = 0''.0870$ (YPC) is slightly more massive than the 1.65 $M_\odot$ model. From the published estimate of the error in the parallax one can estimate a reasonable range of masses for η Boo. But, as we describe below, some of these models are inconsistent with reasonable values of the Galactic-enrichment parameter $\Delta Y/\Delta Z$; hence, even more stringent constraints can be applied.

TABLE 7

PARALLAX, RADIUS, LUMINOSITY FOR η BOO

Parallax	$R/R_\odot$	$L/L_\odot$
0".0858.....	2.806	9.452
0.0870.....	2.767	9.193
0.0882.....	2.730	8.945
0.0894.....	2.693	8.706
0.0906.....	2.657	8.477
0.0918.....	2.622	8.257

As mentioned in § 2.4, known errors in modeling the very surface layers in the superadiabatic region of the Sun introduce a nonzero slope in frequency-difference plots (i.e., the frequency spacing is not correct). This is primarily because the mixing-length formalism used in the models fails to realistically describe the transition superadiabatic layer in the subphotosphere (see, e.g., Kim et al. 1995). We expect that the surface layers of η Boo are just as poorly determined, and, hence, we also expect the frequency spacing or, equivalently, the lines of common l-values in the frequency-difference plots to show a nonzero slope. In the case of the Sun, the slope is positive, the opposite of that shown for η Boo. This makes η Boo an important target for future research on the surface layers of the Sun and stars using the tools of seismology.

Assuming the frequencies have been calculated to an accuracy of ± 5 μHz, then for a given parallax and metallicity, the observed p-mode frequencies constrain the mass to an accuracy of ± 0.03 $M_\odot$. Comparing Figures 3–5 with Figure 2, it is clear that the p-mode frequencies do depend on the metallicity and the mixing-length parameter, with the greatest sensitivity demonstrated for Z.

Comparing Figure 6 with Figure 2, we see that the OPAL equation of state has an insignificant (less than 1 μHz) effect on the p-mode frequencies. Although the OPAL equation of state does improve the modeling of the hydrogen and helium ioniza-

tion regions and more accurately deals with the Coulomb corrections in the core, the observed low-l p-modes are relatively insensitive to these layers.

The second-order spacing, $\delta_{n,l} \equiv \nu_{n,l} - \nu_{n-1,l+2}$, is sensitive to the deep interior and, hence, is sensitive to the evolutionary age of the model. All of the models reproduce the observed second-order spacing reasonably well. This is seen by the nearly perfect overlap and near-horizontal slope of the $l = 0$ and 2 lines (the shorter length lines) in the frequency-difference plots. The second-order spacing of the models is within 10% of the observed second-order spacing; the spacing is too small for most of the models.

3.3. *Mode Bumping*

The p-mode frequencies of η Boo are not as regularly spaced as they are for the Sun, and it has been suggested that this may be a consequence of mode bumping (KBVF; CBK). Our calculations, as expected, produce similar behaviour. As η Boo evolves off the main sequence, nuclear burning depletes hydrogen in the core, replacing it with helium. This produces a steep molecular weight gradient located just outside the core. The μ-gradient provides a barrier within which g-modes can be trapped. Those g-modes whose frequencies overlap the frequencies of p-modes will perturb the frequencies of the p-modes. A p-mode in the overlapping part of the spectrum will have both g-mode character (in the central regions) and p-mode character (in the outer regions) (see Guenther 1991). This subject is well studied for massive stars, such as β Cephei variable stars, where the μ-gradient is left behind by the retreating edge of the convective core (Aizenman, Smeyers, & Weigert 1977; Scuflaire 1974; Shibahashi 1979; Christensen-Dalsgaard 1981; Osaki 1975; Gabriel 1980).

Mode bumping is like a beating phenomenon and, in principle, can be used to fine-tune the models of η Boo. Very small changes to the age of the model will produce large changes to the amount the frequency of a particular p-mode is perturbed by mode bumping. Once one is confident that a model of η Boo is close to the actual structure of η Boo, it should be possible to fine-tune the age of the model by reproducing the observed mode-bumping signature.

The effects of mode bumping are visible in Figures 2–6. Consider the $\pi = 0''.0870$ plot in Figure 2. The frequencies of the modes of the 1.70 $M_\odot$ model, for example, do not *all* show the same systematic differences. In other words, the data points are not collinear. The $l = 1$, $n = 18$ mode (the second point from the left among the longest line in Fig. 2) is perturbed by ~ 10 μHz from where one would expect it to fall. Plots of the original data in KBVF show that this mode and the $l = 1$, $n = 17$ mode are perturbed, in the sense that they are not regularly spaced in frequency between neighboring modes. If a model of η Boo reproduces the observed bumping, then the frequencies of the modes will appear to line up in the frequency-difference plots. When they do not, as in the example cited, it indicates that the mode bumpings are not perfectly matched. The p-mode frequencies of the 1.65 $M_\odot$ model (Fig. 2, $\pi = 0''.0870$ plot), on the other hand, do nicely reproduce the mode-bumping characteristics that are observed. At this time, we cannot constrain the physical characteristics of the model of η Boo precisely enough to be confident in trying to fine-tune the model using the mode-bumping signature. Here we do note that we can reproduce the mode-bumping signature for some of our models of η Boo. This, in our opinion, is strong evidence supporting the real identification of p-modes on η Boo.

3.4. *Detailed Analysis with All Constraints*

In order to simplify the analysis of the data, we have selected a single mode, the $l = 0$, $n = 20$ mode (see Tables 2–6), from the set of modes calculated for each model to represent the p-mode frequencies of that model. In Figures 7–11 we plot the calculated frequency against the mass of the model. Models constructed using the same assumed parallax are connected by a line. To the right of each data point is the value of $\Delta Y/\Delta Z$ for that model. Dashed lines approximately identify, in the plot, where $\Delta Y/\Delta Z = 1.5$ and $\Delta Y/\Delta Z = 3.5$, and hence define the region in which acceptable values of the Galactic-enrichment parameter of the models are located. A thick-lined trapezoid defines a region intersecting $1.5 \leq \Delta Y/\Delta Z \leq 3.5$ and 848.7 $\mu\text{Hz} \leq \nu \leq 858.7$ μHz. The latter constraint is ± 5 μHz around the observed frequency of the $\nu(l = 0,\ n = 20)$ p-mode. The trapezoids, therefore, define outside limits on acceptable values for the frequency of the $\nu(l = 0,\ n = 20)$ p-mode and the Galactic-enrichment parameter.

It is clear from Figure 11 ($Z = 0.03$, $\alpha = 1.7$, OPAL equation of state) that the best set of values for the mass and parallax of η Boo are $M = 1.55 \pm 0.03$ $M_\odot$ and $\pi = 0''.0895 \pm 0''.0005$, where the errors reflect uncertainties in the model-frequency determination and the Galactic-enrichment parameter. The implied parallax is just within the error range of the observed parallax for η Boo ($\pi = 0''.0870 \pm 0''.034$).

It is not assured that η Boo requires the same mixing-length parameter as the Sun, although isochrone calculations (Chaboyer et al. 1995; Dinescu et al. 1995) indicate our adopted value of $\alpha = 1.7$ is optimum for our choice of input physics. To see how big an effect a different mixing length will have on the p-mode frequencies, we have calculated a set of models assuming $\alpha = 2.0$ (with $Z = 0.03$). The resultant frequency versus mass plot, Figure 8, shows that increasing the mixing-length parameter shifts the error trapezoid slightly to higher masses and lower parallaxes when compared to the benchmark models in Figure 7. Increasing the mixing-length parameter from $\alpha = 1.7$ to $\alpha = 2.0$ increases the model-determined mass by $+0.02$ $M_\odot$ and decreases the model-determined parallax by $0''.007$. The YPC parallax still appears to be too low.

To show what effect the uncertainties in the abundance determination will have on our results, we have tested Z values ranging from $Z = 0.02$ to $Z = 0.04$. In Figures 9 and 10 we show the shift in the error trapezoid for models with $Z = 0.02$ and $Z = 0.04$, respectively ($\alpha = 1.7$). Here the effect of uncertainty in Z on implied mass is much greater. Decreasing Z from $Z = 0.03$ to $Z = 0.02$ decreases the mass (compared to the benchmark models in Fig. 7) by 0.13 $M_\odot$ and increases the parallax by $\pi = 0''.025$. Increasing Z from $Z = 0.03$ to $Z = 0.04$ increases the mass (compared to the benchmark models is Fig. 7) by 0.10 $M_\odot$ and decreases the parallax by $\pi = 0''.023$. The uncertainty in Z is about one-half the range presented here. Regardless, the uncertainty in Z is the largest source of uncertainty with regard to using seismology to determine the mass of η Boo, introducing an uncertainty of ± 0.06 $M_\odot$.

By fixing the mass of η Boo based on the frequency versus mass plots (and Galactic chemical enrichment) one also constrains the age and helium abundance of the models. For example, the best models ($Z = 0.03$, $\alpha = 1.7$, and OPAL equation of state), when constrained by seismology and $\Delta Y/\Delta Z$,

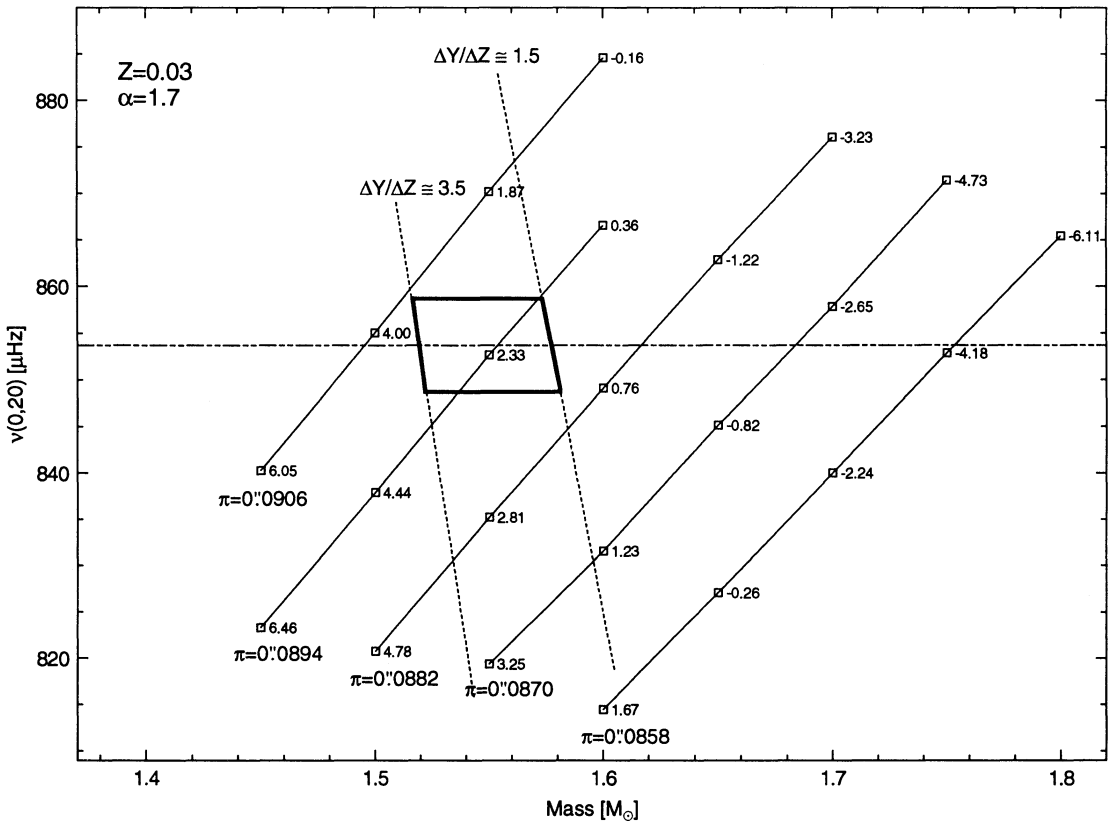

FIG. 7.—Frequencies of the $\nu(l = 0, n = 20)$ p-mode for different models of η Boo are plotted against the mass of the model. Solid lines connect models constructed with the same assumed parallax. Each data point is labeled by the Galactic-enrichment parameter $\Delta Y/\Delta Z$ for that model. All of the models shown were constructed with $Z = 0.03$ and $\alpha = 1.7$.

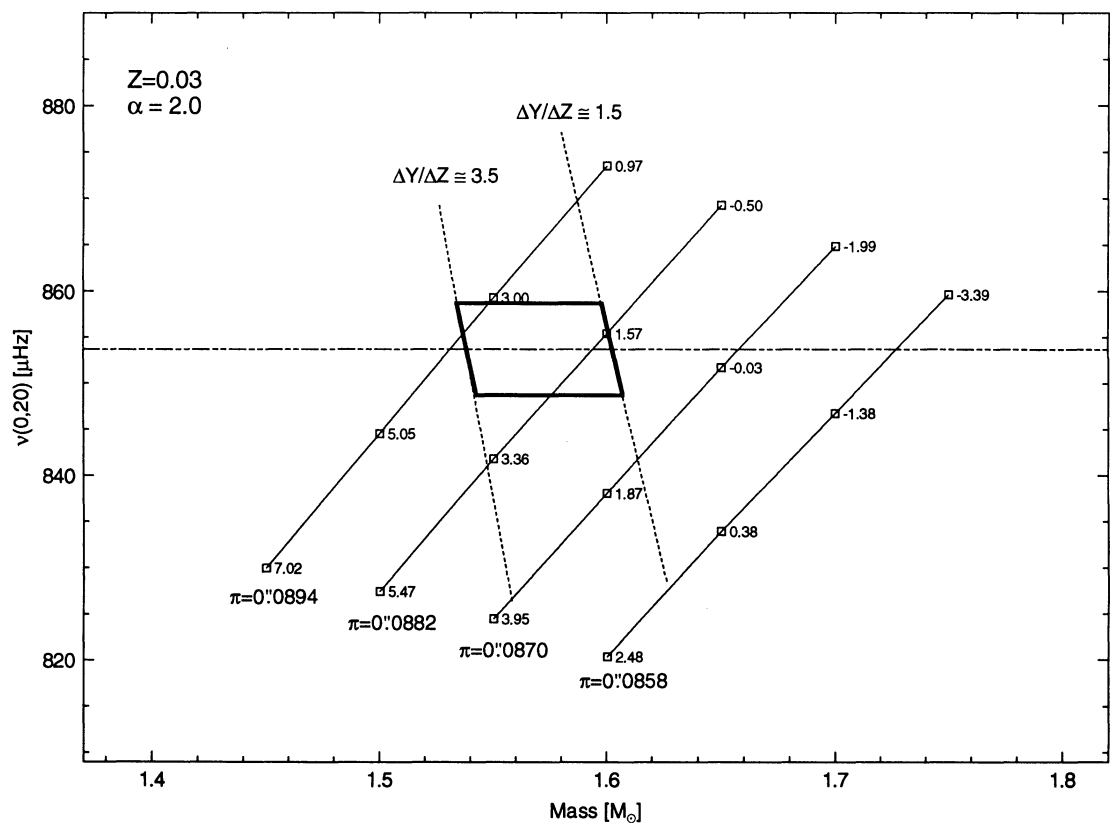

FIG. 8.—Similar to Fig. 7, except that models were constructed with $Z = 0.03$ and $\alpha = 2.0$

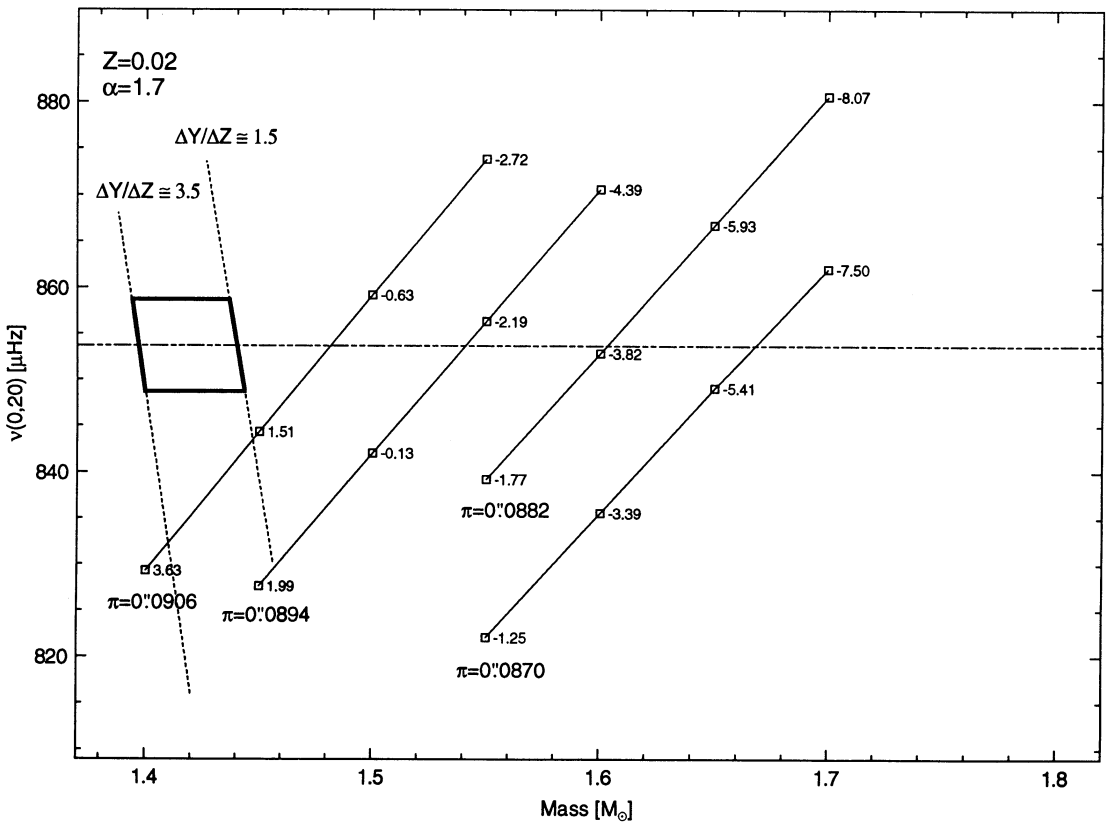

FIG. 10.—Similar to Fig. 7, except that models were constructed with $Z = 0.04$ and $\alpha = 1.7$

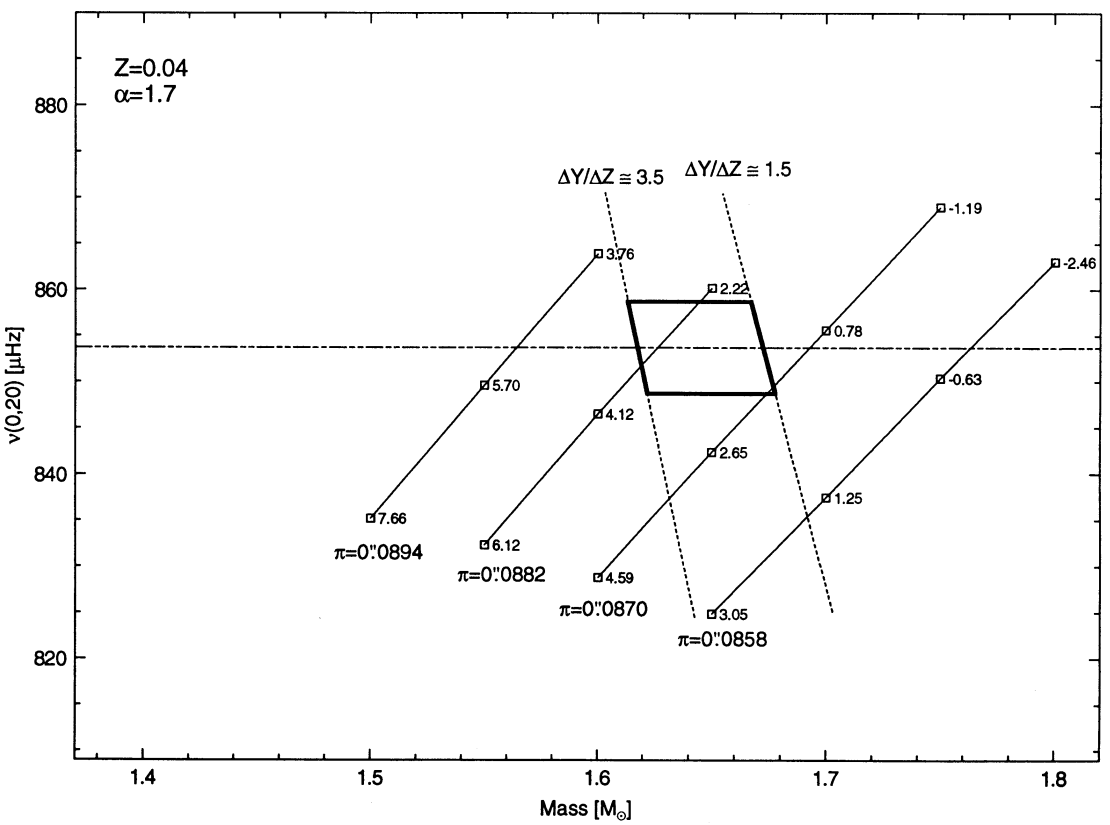

FIG. 9.—Similar to Fig. 7, except that models were constructed with $Z = 0.02$ and $\alpha = 1.7$

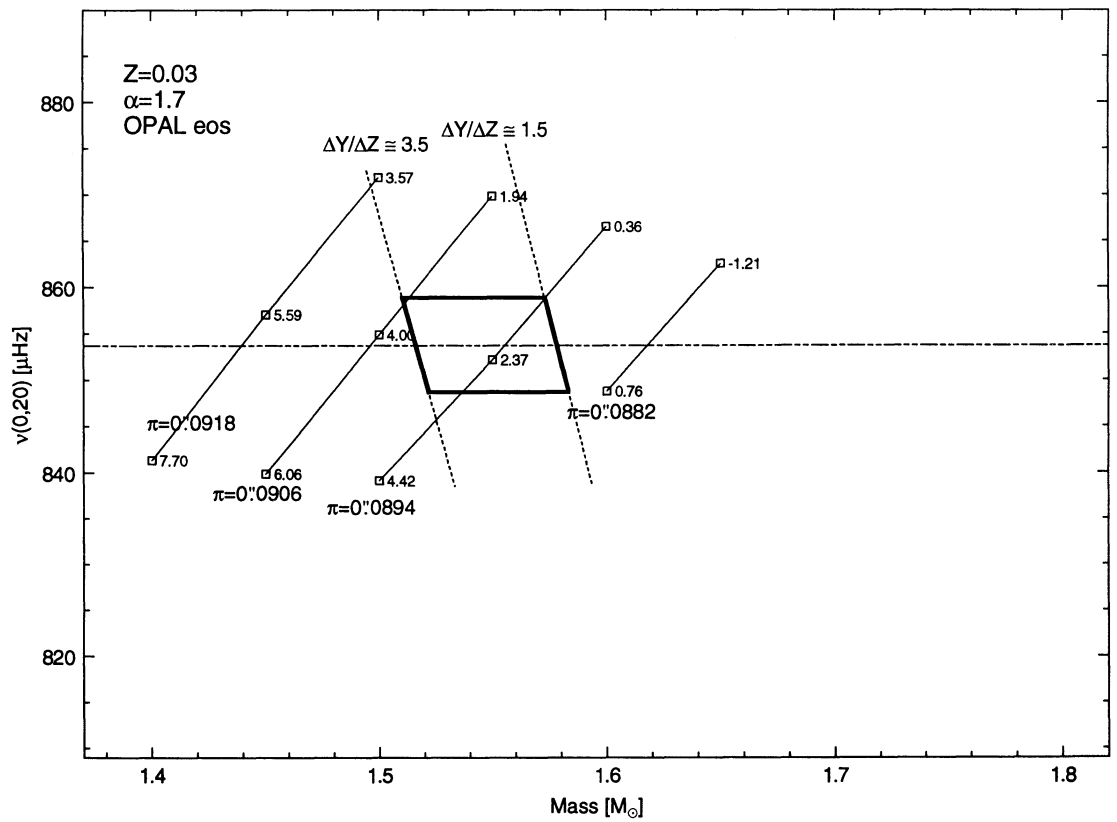

FIG. 11.—Similar to Fig. 7, except that models were constructed using the latest OPAL equation-of-state routines (with $Z = 0.03$ and $\alpha = 1.7$)

yield a value of $M = 1.55 \pm 0.03\ M_\odot$ and $\pi = 0''.0895 \pm 0''.0005$. From Table 6 we see that this corresponds to a star with an age ~ 2.3 Gyr and a surface helium abundance $Y = \sim 0.28$.

In the spirit of Brown (1991), one could have adopted a rigorous approach where the oscillation-mode spectrum is used to reduce the size of the error volume associated with all of the observables. We have chosen a less formal approach because it provides more insight into the interplay of the various uncertainties in the stellar evolution observables and the oscillation spectrum. More important, we have cast our results in such a way as to enable the reader to infer directly from our tables and diagrams the effect of any future improvements in the most critical input parameters, i.e., the metallicity and the parallax.

4. SUMMARY AND CONCLUSIONS

Inspired by the impressive results of KBVF, who, for the first time, make a plausible case for measuring the p-mode spectrum of a Sun-like star we explore in this paper some tests of stellar structure theory which we derive from observations of stellar p-modes combined with other astronomical measurements.

A grid of stellar evolutionary sequences tuned to match the position of η Boo in the theoretical H-R diagram have been constructed for the range in trigonometric parallax quoted in the YPC, and for the range in metallicity derived from spectroscopic observations. Given a value of the parallax and the metallicity, a fit in the H-R diagram yields a family of models for η Boo. Each model yields a consistent helium content Y, mass, and age for η Boo. We find that all models show that η Boo has exhausted hydrogen in its core and is in the shell-narrowing phase evolving toward the giant branch (consistent with its spectral classification as a G0 subgiant).

The low-l p-mode spectrum has been calculated for each model in the family of models which fit η Boo's position in the H-R diagram and satisfy its metallicity constraint. Reasonable stellar models of η Boo can be constructed that reproduce the observed spectrum. Possibly of greater significance, some of the models reproduce the observed mode bumpings. This stringent test can only be satisfied if the stellar models and η Boo are in nearly identical phases of evolution—small perturbations to the models greatly affect the signature of the mode bumpings.

Our results reveal the high sensitivity of the p-mode spectrum to the helium abundance and mass of the model. The p-modes provide a tighter constraint on η Boo's distance than the trigonometric parallax, which lies just inside the limits of the weighted standard error of the YPC parallax.

Our OPAL equation-of-state–based models yield a mass $M = 1.55\ M_\odot$, a parallax of $\pi = 0''.0895$, an age of ~ 2.3 Gyr, and a surface helium abundance $Y = \sim 0.28$. The uncertainty in the Galactic-enrichment parameter $\Delta Y/\Delta Z = 1.5$–3.5 and the frequency calculation $\pm 5\ \mu$Hz introduces an uncertainty in the mass and the parallax of $\pm 0.03\ M_\odot$ and $\pm 0''.0005$, respectively. Additionally, the uncertainty in the observed value of $Z = 0.025$–0.035 introduces an uncertainty in the mass and the parallax of $\pm 0.06\ M_\odot$ and $\pm 0''.001$, respectively.

The choice of equation of state does not affect the mass and parallax of the optimum model for η Boo. Going from our standard equation-of-state routines to the new OPAL equation-of-state routines (F. J. Rogers 1995, private communication) decreases the mass in the convection zone, but

does not perturb the p-mode frequencies (corresponding to the observed modes) by more than 1 μHz.

We note that when the p-mode data are taken into account, the helium content Y, through the parameter $\Delta Y/\Delta Z$, also provides a constraint on the solution. Remarkably, requiring that $1.5 \leq \Delta Y/\Delta Z \leq 3.5$, a very weak statement from the point of view of Galactic nucleosynthesis, restricts the parallax to the range $\pi = 0''.0895 \pm 0''.0005$ ($Z = 0.03$, $\alpha = 1.7$, and OPAL equation of state). Very clearly, the long-awaited results from *HIPPARCOS*, with an expected parallax precision of 2 mas, will severely test our theoretical models of η Boo and the conclusions of this paper.

We find that the principal source of uncertainty investigated here is η Boo's metallicity. If the observed parallax is correct ($\pi = 0''.0870 \pm 0''.034$), then the models suggest that the adopted metallicity ([Fe/H] = 0.19 or $Z = 0.03$) may be too low; models for $Z = 0.04$ ([Fe/H] = 0.33) will yield better agreement with the observed p-mode frequencies. This high sensitivity to the metallicity and the parallax highlights the special advantage that observing stars in binary systems or in clusters would have because one could assume a common chemical composition, distance, and age.

Further observations of η Boo will be needed to confirm the KBVF identifications of p-modes and to refine their frequencies. In our opinion, the consistencies of the observed frequencies with theoretical predictions, and especially the presence of mode bumping, as expected in a subgiant star with a hydrogen-exhausted core in η Boo's position in the H-R diagram, leave little room for doubting the reality of these observations. This point, already made by CBK, is underscored by our analysis. Even if it turns out that some of the modes identified by KBVF are not real, the methodology that we outline here can still yield unique information about η Boo. Our study further illustrates the enormous potential of seismology, when combined judiciously with improved spectroscopic abundances and parallax measurements, for testing the validity of the theory of stellar structure and evolution, and its applications to Galactic astronomy.

We thank Y.-C. Kim for his implementation of the OPAL equation of state in YREC, and J. T. Lee and E. Horch for their help and advice on the astrometric data. The authors gratefully acknowledge support for this research from NSERC (D. B. G.), and from NASA grants NAG 5-1486 and NAG 5-2795 (P. D.).

REFERENCES

Aizenman, M., Smeyers, P., & Weigert, A. 1977, A&A, 58, 41
Anders, E., & Grevesse, N. 1989, Geochim, Cosmochim. Acta, 53, 197
Bahcall, J. N. 1989, Neutrino Astrophysics (Cambridge: Cambridge Univ. Press)
Bahcall, J. N., Bahcall, N. A., & Shaviv, G. 1968, Phys. Rev. Lett., 20, 1209
Bahcall, J. N., & Pinsonneault, M. H. 1992, Rev. Mod. Phys., 64, 885
Balmforth, N. J. 1992a, MNRAS, 255, 603
———. 1992b, MNRAS, 255, 632
———. 1992c, MNRAS, 255, 639
Batten, A. H., Fletcher, J. M., & MacCarthy, D. G. 1989, Eighth Catalogue of the Orbital Elements of Spectroscopic Binary Systems (Publ. Dorn. Astrophys. Obs., Vol. 17; NRC 29684)
Bell, R. A., & Gustafsson, B. 1989, MNRAS, 236, 653
Bertiau, F. C. 1957, ApJ, 125, 696
Blackwell, D. E., & Lynas-Gray, A. E. 1994, A&A, 282, 899
Bressan, A., Chiosi, C., & Fagotto, F. 1994, ApJS, 94, 63
Brown, T. M. 1991, in ASP Conf. Ser. 20, Frontiers of Stellar Evolution, ed. D. L. Lambert (San Francisco: ASP), 139
Chaboyer, B., Demarque, P., Guenther, D. B., & Pinsonneault, M. H. 1995, ApJ, 446, 435
Chaboyer, B., Demarque, P., Guenther, D. B., Pinsonneault, M. H., & Pinsonneault, L. L. 1995, in The Formation of the Milky Way, ed. E. J. Alfaro & G. Tenorio-Tagle (Cambridge: Cambridge Univ. Press), in press
Christensen-Dalsgaard, J. 1981, MNRAS, 194, 229
Christensen-Dalsgaard, J., Bedding, T. R., & Kjeldsen, H. 1995, ApJ, 443, L29 (CBK)
Clayton, D. 1968, Principles of Stellar Evolution and Nucleosynthesis (New York: McGraw-Hill)
Cox, J. P., & Giuli, R. T. 1968, Principles of Stellar Structure (New York: Gordon & Breach)
Demarque, P., Guenther, D. B., & van Altena, W. F. 1986, ApJ, 300, 773
Dinescu, D., Demarque, P., Guenther, D. B., & Pinsonneault, M. H. 1995, AJ, 109, 2090
Edmonds, P., Cram, L., Demarque, P., Guenther, D. B., & Pinsonneault, M. H. 1992, ApJ, 394, 313
Edvardsson, B., Andersen, J., Gustafsson, B., Lambert, D. L., Nissen, P. E., & Tomkin, J. 1993, A&A, 275, 101
Gabriel, M. 1980, A&A, 82, 8
Guenther, D. B. 1987, ApJ, 312, 211
———. 1991, ApJ, 375, 352
———. 1994, ApJ, 442, 400
Guenther, D. B., & Demarque, P. 1986, ApJ, 301, 207
———. 1993, ApJ, 405, 298
Guenther, D. B., Demarque, P., Kim, Y.-C., & Pinsonneault, M. H. 1992, ApJ, 387, 372
Guenther, D. B., Jaffe, A., & Demarque, P. 1989, ApJ, 345, 1022
Guenther, D. B., Kim, Y.-C., & Demarque, P. 1995, ApJ, in press
Harrington, R. S., et al. 1993, AJ, 105, 1571
Hoffleit, D., & Jaschek, C. 1982, The Bright Star Catalogue (4th rev. ed.; New Haven: Yale Univ. Obs.)
Iglesias, C. A., & Rogers, F.J. 1991, ApJ, 371, 408
Kim, Y.-C., Fox, P. A., Sofia, S., & Demarque, P. 1995, ApJ, 442, 422
Kjeldsen, H., Bedding, T. R., Viskum, M., & Frandsen, S. 1995, AJ, 109, 1313 (KBVF)
Kurucz, R. L. 1991, in Stellar Atmospheres: Beyond Classical Models, ed. L. Crivellari, I. Hubeny, & D. G. Hummer (Dordrecht: Kluwer), 440
Landau, E. M., & Lifshitz, E. M. 1959, Statistical Physics (Oxford: Pergamon)
McAllister, H. A., & Hartkopf, W. I. 1988, Second Catalog of Interferometric Measurements of Binary Stars (Atlanta: Georgia State Univ.)
Osaki, Y. 1975, PASJ, 27, 237
Rogers, F. J., & Iglesias, C. A. 1994, Science, 263, 50
Rogers, F. J., Swenson, F. J., & Iglesias, C. A. 1995, 456, 000
Scuflaire, R. 1974, A&A, 36, 107
Shibahashi, H. 1979, PASJ, 31, 87
Soderblom, D., & Däppen, W. 1989, ApJ, 342, 945
Tomkin, J., Lambert, D. L., & Balachandran, S. 1985, ApJ, 290, 289
van Altena, W. F., Lee, J. T., & Hoffleit, D. 1995, The General Catalogue of Trigonometric Parallaxes (New Haven: Yale Univ. Obs.) (YPC)